Re-examination of analytical models for microwave scattering from deciduous leaves

Y. Oh and J.-Y. Hong

Abstract: This paper presents an examination of classical scattering models for radar cross sections of deciduous leaves, such as the generalised Rayleigh-Gans (GRG) model and the physical optics (PO) model. The PO model employs the resistive sheet approximation in this study. The validity regions of the analytical models for microwave scattering from deciduous leaves are investigated by comparison with the precise numerical results of the method of moment. It was found that the GRG and PO models extend their validity regions for estimating the scattering amplitudes as the thickness of a lossy dielectric disk decreases. The GRG and PO models can be used alternatively for computing the scattering matrices of natural deciduous leaves at microwave frequencies regardless of the size of the leaves, because of the very small thickness of the leaves (0.2–0.4 mm).

1 Introduction

The radiative transfer theory has been commonly used in computations of microwave backscatter from vegetation canopy for radar applications [1, 2] and microwave propagation through vegetation for designing wireless communication services [3]. It is necessary to precisely compute the scattering matrices of leaves at microwave frequencies to compute the phase and extinction matrices of the crown layer. A deciduous leaf larger or comparable to a wavelength has been usually modelled as a randomly oriented dielectric resistive sheet and the scattering matrix of this leaf has been computed using the physical optics (PO) model [4]. On the other hand, the scattering matrix of a deciduous leaf smaller or comparable to a wavelength has commonly been computed using the generalised Rayleigh-Gans (GRG) model [5].

The interior field in the PO approach is assumed to be the same as that of an infinite disk, which is often considered to be only valid at high microwave frequencies for natural leaves. In the GRG approach, the electric field inside the dielectric disk is approximated by the incident electric field, which is often considered to be valid in low microwave frequencies. The radar cross section (RCS) of a dielectric sheet was computed using these models and compared with the method of moments (MoM) with an approximate boundary condition at 1 and 10 GHz [6, 7]. Frequency limitations of the analytic scattering models need to be examined for dielectric disks having dimensions of natural leaves. The GRG and PO approximations for elliptical and circular dielectric disks are reviewed inceptively. Then, a full-wave analysis with the MoM [8] is performed to examine the accuracy of both analytical scattering models.

Fig. 1 shows a coordinate system of the scattering problem with a plane wave incidence on an elliptical dielectric disk lying on the $x-y$ plane and the forward scattering assignment as in [9] with $\hat{k}_i = \sin\theta_i\cos\phi_i\hat{x} + \sin\theta_i\sin\phi_i\hat{y} + \cos\theta_i\hat{z}$, $\hat{h}_i = \hat{z}\times\hat{k}_i/|\hat{z}\times\hat{k}_i|$, $\hat{v}_i = \hat{h}_i\times\hat{k}_i$ and $(\hat{v}_s, \hat{h}_s, \hat{k}_s)$, which can be obtained from $(\hat{v}_i, \hat{h}_i, \hat{k}_i)$ by substituting i's with s's.

A volume current density $\bar{J}(\bar{r})$ is induced in the dielectric disk with an incident electric field of

$$\bar{E}^i(\bar{r}) = \hat{q}_i E_0\ \mathrm{e}^{ik\hat{k}_i\cdot\bar{r}} \tag{1}$$

where $\hat{q}_i = \hat{v}_i$ for a vertically polarised incidence wave or $\hat{h}_i$ for a horizontally polarised incidence wave, k is the wavenumber of the incidence wave, $\bar{r}$ is a position vector at an observation point and a time convention of $\exp[-\mathrm{i}\omega t]$ is assumed. Then, the electric fields scattered from the dielectric body are computed using the electric current density $\bar{J}(\bar{r}')$ and the dyadic Green's function $\bar{\bar{G}}(\bar{r}, \bar{r}')$ by

$$\bar{E}^s(\bar{r}) = ik_0\eta_0\int_V \bar{\bar{G}}(\bar{r}, \bar{r}')\cdot\bar{J}(\bar{r}')\,\mathrm{d}v' \tag{2}$$

where $k_0 = 2\pi/\lambda_0$ and $\eta_0 = \sqrt{(\mu_0/\varepsilon_0)}$. The dyadic Green's function is given as in [10]

$$\bar{\bar{G}}(\bar{r}, \bar{r}') = \left(\bar{\bar{I}} + \frac{\nabla\nabla}{k^2}\right)G(\bar{r}, \bar{r}') \tag{3}$$

where $\bar{\bar{I}}$ is an identity dyad, and

$$G(\bar{r}, \bar{r}') = \frac{\mathrm{e}^{ik|\bar{r}-\bar{r}'|}}{4\pi|\bar{r}-\bar{r}'|} \tag{4}$$

In the far field, the scattered fields can be calculated with the following approximated equations

$$\bar{\bar{G}}(\bar{r}, \bar{r}') \simeq (\hat{v}_s\hat{v}_s + \hat{h}_s\hat{h}_s)\frac{\mathrm{e}^{ikr}}{4\pi r}\mathrm{e}^{-ik\hat{k}_s\cdot\bar{r}'} \tag{5}$$

The current density $\bar{J}(\bar{r}')$ in the dielectric disk is obtained in a simple form with appropriate assumptions for the analytical models (the GRG and the PO approximations) in Section 2, whereas $\bar{J}(\bar{r}')$ is computed precisely applying the MoM on an integral equation derived by using (2), (3) and (4) for a full-wave analysis in Section 3. Then, the scattered fields are computed using (2) and (5) for the analytical

© The Institution of Engineering and Technology 2007

doi:10.1049/iet-map:20050081

Paper first received 12th April 2005 and in revised form 20th July 2006

The authors are with the School of Electronic and Electrical Engineering, Hongik University, Seoul, Korea

E-mail: yisokoh@hongik.ac.kr

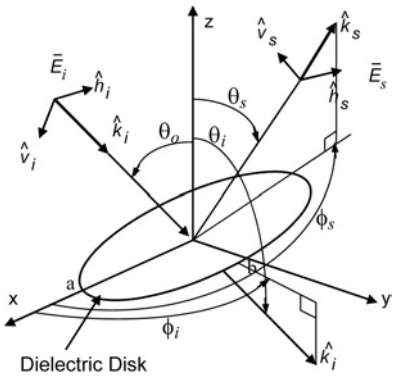

Fig. 1 *Coordinate system of the scattering problem*

and numerical models. Because of the very small thickness of a deciduous leaf, the MoM technique employs a very thin brick grid. The accuracy of the MoM technique with the thin cells is verified in Section 3. In Section 4, the scattering amplitudes of various leaves are computed by the analytical models and compared with the full-wave method. Then, the accuracy of each analytical model is investigated in microwave frequencies using the precise numerical results.

2 Analytical models

In this section, the formulae of the GRG and PO models are briefly introduced. For the GRG model, the internal field within the dielectric disk is assumed to be the same as the incidence field assuming the leaf size is lesser than a wavelength ($ka \ll 1$), and the phase interference of the scattering is retained. For the PO approximation, the edge effect is ignored assuming that the leaf size is much greater than a wavelength. Moreover, the thin leaf can be assumed to be a resistive sheet.

The scattered field vector is related to the incident field vector in terms of a dyadic scattering matrix $\bar{\bar{S}}$ as follows

$$\bar{E}^s(\bar{r}) = \frac{e^{ikr}}{r}\bar{\bar{S}}(\hat{k}_s, \hat{k}_i)\cdot\hat{q}_i E_0 \tag{6}$$

where the scattering amplitudes, which are elements of the scattering matrix, S_{pq} for a q-polarised incident wave and a p-polarised scattered wave can be written by

$$S_{pq} \equiv \hat{p}_s \cdot \bar{\bar{S}}(\hat{k}_s, \hat{k}_i)\cdot\hat{q}_i \tag{7}$$

Then, the RCS of the dielectric disk is computed by

$$\sigma_{pq} = 4\pi|S_{pq}|^2 \quad p, q = v, h \tag{8}$$

2.1 GRG approximation

Assuming the disk is very small relative to a wavelength, the field inside the disk is approximated to the incident field $\bar{E}^i(\bar{r}')$. Then, the scattering amplitude is given in [11] as follows

$$S_{pq} = \hat{p}_s \cdot \frac{k^2}{4\pi}(\varepsilon_r - 1)(\hat{v}_s\hat{v}_s + \hat{h}_s\hat{h}_s)\cdot\bar{\bar{A}}\cdot\hat{q}_i M(\hat{k}_s, \hat{k}_i) \tag{9}$$

for a $\hat{q}$-polarised incident wave and a $\hat{p}$-polarised scattered wave where $\hat{q}_i = \hat{v}_i$ or $\hat{h}_i$, and $\hat{p}_s = \hat{v}_s$ or $\hat{h}_s$. The polariability tensor $\bar{\bar{A}}$ is given in [11, 12] as

$$\bar{\bar{A}} = \frac{\hat{x}\hat{x}}{1+(\varepsilon_r-1)g_1} + \frac{\hat{y}\hat{y}}{1+(\varepsilon_r-1)g_2} + \frac{\hat{z}\hat{z}}{1+(\varepsilon_r-1)g_3} \tag{10}$$

The demagnetising factors, $g_i (i = 1-3)$, can be written for an elliptic disk-shaped leaf ($a > b \gg (t/2)$) as

$$g_1 = \frac{t}{2a}\sqrt{1-e^2}\,\frac{K(e)-E(e)}{e^2} \tag{11a}$$

$$g_2 = \frac{t}{2a}\,\frac{E(e)-(1-e^2)K(e)}{e^2\sqrt{1-e^2}} \tag{11b}$$

$$g_3 = 1 - \frac{t}{2a}\,\frac{E(e)}{\sqrt{1-e^2}} \tag{11c}$$

with $e = \sqrt{(1-(b/a)^2)}$. $K(e)$ and $E(e)$ are the elliptic integrals of the first and second kind, respectively, and can be computed with polynomial approximations as in [13].

The modifying factor M can be obtained by integrating the phase term $\exp[ik(\hat{k}_i - \hat{k}_s)\cdot\bar{r}']$ over the volume of a dielectric oblate spheroid, with a couple of integral transformations

$$M(\hat{k}_s, \hat{k}_i) = 2\pi abt\int_0^1 J_0(Q\lambda)\lambda\,d\lambda = 2\pi abt\frac{J_1(Q)}{Q} \tag{12}$$

where t is the thickness of the disk, $Q = \sqrt{((k_x a)^2 + (k_y b)^2)}$, $k_x = k(\hat{k}_i - \hat{k}_s)\cdot\hat{x}$ and $k_y = k(\hat{k}_i - \hat{k}_s)\cdot\hat{y}$. Fig. 2 shows the cross section of a dielectric oblate spheroid with a, b and c.

2.2 PO approximation

The equivalent current density $\bar{J}(\bar{r}')$ in (2) can be approximated to a surface current distribution $\bar{J}_s^R(\bar{r}')$ [4] on the resistive sheet lying on an $x-y$ plane as

$$\bar{J}_s^R(\bar{r}') = \bar{J}_s^{pc}(\bar{r}')\Gamma_q \tag{13}$$

where $\bar{J}_s^{pc}\bar{r}'$ is the PO surface current of a perfect conductor. The horizontal and vertical reflection coefficients (Γ_h and Γ_v) for a resistive sheet can be derived using the impedance boundary conditions as in [4]

$$\Gamma_h = \left[1 + \frac{2R\cos\theta_0}{\eta_0}\right]^{-1} \text{and} \quad \Gamma_v = \left[1 + \frac{2R}{\eta_0\cos\theta_0}\right]^{-1} \tag{14}$$

with

$$R = \frac{i\eta_0}{k_0 t(\varepsilon_r - 1)} \tag{15}$$

where R is the resistivity of the leaf, $\theta_0 = \pi - \theta_i$, and t is the leaf thickness.

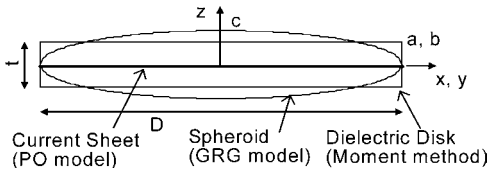

Fig. 2 *Cross sections of a dielectric slab for the analytical models and the MoM*

The scattering amplitude for a $\hat{q}$-polarised incident wave and a $\hat{p}$-polarised scattered wave is given as

$$S_{pq} = \hat{p}_s \cdot \frac{ik}{2\pi}(\hat{v}_s\hat{v}_s + \hat{h}_s\hat{h}_s) \cdot [\hat{z} \times (\hat{k}_i \times \hat{q}_i)]\Gamma_q m(\hat{k}_s, \hat{k}_i) \quad (16)$$

where the phase interference function $m(\hat{k}_s, \hat{k}_i)$ is the same with $M(\hat{k}_s, \hat{k}_i)$ in (12) except the multiplying factor t. For example, S_{vh} can be computed by substituting $\hat{h}_i$ into $\hat{q}_i$ and $\hat{v}_s$ into $\hat{p}_s$ presented in (16).

3 Full-wave analysis

3.1 Formulation

At first, we obtain the equivalent volume current $\bar{J}(\bar{r}')$ in the dielectric disk as

$$\bar{J}(\bar{r}') = -i\omega\varepsilon[\varepsilon_r - 1]\bar{E}(\bar{r}') \quad (17)$$

from the Maxwell equations, where ε_r is the complex dielectric constant of the disk and $\bar{E}(\bar{r}')$ is the total electric field including the incident and scattered fields, $\bar{E} = \bar{E}^i + \bar{E}^s$. Then, an integral equation can be obtained by substituting (2) into (17) as

$$\bar{J}(\bar{r}) - k_0^2(\varepsilon_r - 1)\int_V \bar{\bar{G}}(\bar{r}, \bar{r}') \cdot \bar{J}(\bar{r}')\,dv' = -i\omega\varepsilon(\varepsilon_r - 1)Ei(\bar{r}) \quad (18)$$

The unknown current density $\bar{J}(\bar{r})$ in the leaf can be computed numerically using the MoM. Among many other basis functions, the volumetric brick was chosen as the basis function for simplicity in the limit of electrically small subdomains. Using the point matching technique, the integral equation (18) can be cast into the following matrix

$$\begin{bmatrix} [Z_{mn}^{xx}] & [Z_{mn}^{xy}] & [Z_{mn}^{xz}] \\ [Z_{mn}^{yx}] & [Z_{mn}^{yy}] & [Z_{mn}^{yz}] \\ [Z_{mn}^{zx}] & [Z_{mn}^{zy}] & [Z_{mn}^{zz}] \end{bmatrix} \begin{bmatrix} [I_n^x] \\ [I_n^y] \\ [I_n^z] \end{bmatrix} = \begin{bmatrix} [I_n^x] \\ [I_n^y] \\ [I_n^z] \end{bmatrix} = \begin{bmatrix} [V_m^x] \\ [V_m^y] \\ [V_m^z] \end{bmatrix} \quad (19)$$

where I_n^p is an unknown constant of the nth basis function for the p-component of the volume currents ($p = x, y, z$), and

$$V_m^p = -i\omega\varepsilon_0[\varepsilon_r(\bar{r}_m) - 1]\hat{q}\,e^{ik_0\hat{k}_i\cdot\bar{r}_m} \cdot \hat{p} \quad p = x, y, z \quad (20)$$

$$Z_{mn}^{pq} = \delta_{pq}\delta_{mn} - k_0^2[\varepsilon_r(\bar{r}_m) - 1] \times \int_{\Delta V_n} G_{pq}(\bar{r}_m, \bar{r}_n)\,dv_n \quad p, q = x, y, z \quad (21)$$

where δ_{pq} and δ_{mn} are the Kronecker delta functions, and $\bar{r}_m$ and $\bar{r}_n$ represent the mth matching position (observation point) and the nth integration position, respectively. The elements of the dyadic Green's function are found to be

$$G_{pp}(\bar{r}_m, \bar{r}_n) = G(R) + \frac{1}{k_0^2}\frac{\partial^2 G(R)}{\partial p^2} \quad (22a)$$

$$G_{pq}(\bar{r}_m, \bar{r}_n) = \frac{1}{k_0^2}\frac{\partial^2 G(R)}{\partial p\,\partial q} \quad p \neq q \quad (22b)$$

where $p, q = x, y, z$ and $R = |\bar{r}_m - \bar{r}_n|$. Explicit form of differentiations of the Green's functions in (22a) and (22b) are given by

$$\frac{\partial^2 G(R)}{\partial p^2} = G(R)\left\{\frac{p_{mn}^2 f_1}{R^4} - \frac{(1 - ik_0R)}{R^2}\right\} \quad (23a)$$

$$\frac{\partial^2 G(R)}{\partial p\,\partial q} = G(R)\frac{p_{mn}q_{mn}f_1}{R^4} \quad p \neq q \quad (23b)$$

where $p_{mn} \equiv p_m - p_n$, $q_{mn} \equiv q_m - q_n$ and $f_1 = 3 - i3k_0R - k_0^2R^2$.

For a diagonal term of the Z-matrix ($n = m$), the second derivatives of the Green's function $G(R)$ produces the well-known singularity. However, we can avoid this singularity by introducing an auxiliary function $g \equiv 1/4\pi R$ and subdividing the integral region to a small sphere V_ε centred at the observation point and the other part as in [8]

$$\int_{\Delta V_n} G_{pp}\,dv = \int_{\Delta V_n - V_\varepsilon} G_{pp}\,dv + \int_{V_\varepsilon} G\,dv + \frac{1}{k_0^2} \times \left[\int_{V_\varepsilon}\frac{\partial^2}{\partial p^2}(G - g)\,dv + \int_{V_\varepsilon}\frac{\partial^2}{\partial p^2}g\,dv\right] \quad (24)$$

We can evaluate explicitly the integrals in the third and fourth terms of the above equation for a small sphere with radius a, which leads to $-(1 - ika)e^{ika}/3$. The integral of the second term in (24) is also explicitly evaluated and results in $\{-1 + (1 - ika)\,e^{ika}\}/k_0^2$. Therefore (24) becomes

$$\int_{\Delta V_n} G_{pp}\,dv_n = \int_{\Delta V_n - V_\varepsilon} G_{pp}\,dv_n + \frac{1}{k_0^2}\left\{-1 + \frac{2}{3}(1 - ika)e^{ika}\right\} \quad (25)$$

The first integral of the right side of (25) was evaluated using a numerical integration technique. Once the elements of the impedance matrix [**Z**] and the excitation vector [**V**] were calculated, the unknown equivalent volume current [I] inside the dielectric body can be found by inverting (19). Consequently, the scattering amplitude S_{pq} can be computed using (2), (4) and (5).

3.2 Verification

A deciduous leaf can be assumed to be a circular or elliptical dielectric disk with a thickness t of about 0.02–0.04 cm as shown in Fig. 2. The thickness is very small compared to the wavelength; for example, about $\lambda/140$ for 5.3 GHz. If we use cubic cells for the MoM, the size of the matrix for this problem will be very large: for example, 19 600 × 19 600 for a 1λ × 1λ dielectric disk. Therefore we need to use thin-disk-type cells for the MoM computation with precise manipulation. The dielectric constants of the leaf, corresponding to the gravimetric moisture content of Mg (g/cm^3), are obtained from an empirical formula in [14]. For example, $Mg = 0.6$ g/cm^3 corresponds to $\varepsilon_r = (19.2, 6.4)$ at 5.3 GHz.

The first step for the verification of the MoM is to examine the numerical code by comparing the computation results of a simple structure with other computation outputs reported in literature. Fig. 3 shows an excellent agreement among the bistatic scattering RCS computed by this MoM code, simulated by a commercial simulation tool (high-frequency structure simulator), and those reported in [15] for a dielectric cube with a length of $a = \lambda/5$ and a dielectric constant of $\varepsilon_r = 9$.

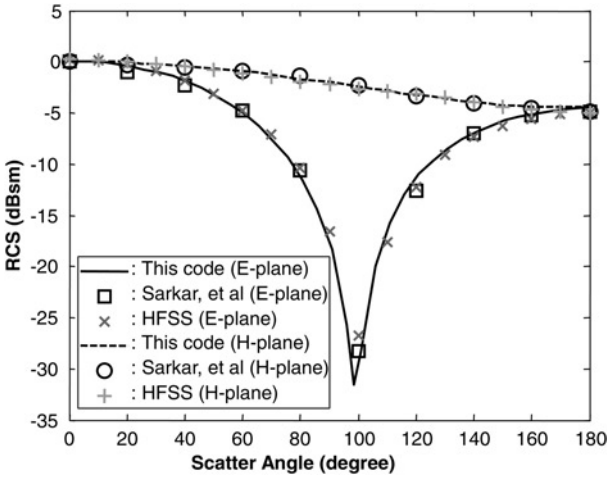

Fig. 3 *Verification of the MoM technique with other numerical results for the RCS of a dielectric*

The second step of the verification is to examine the effect of the cell shape. The numerical integration for the diagonal terms of the impedance matrix elements was optimised with a subdivision technique for thin cells. At first, the forward scatter RCS of a circular disk ($D = 1\lambda$, $t = \lambda/20$ and $\varepsilon_r = 19.2 - j6.4$) with cubic cells ($\lambda/20 \times \lambda/20 \times \lambda/20$) was compared to the RCS with non-cubic cells ($\lambda/20 \times \lambda/20 \times \lambda/40$) at VV- and HH-polarisations. For the latter case, the dielectric disk consists of two layers of $\lambda/40$ -thickness bricks. It was shown that the code is good for non-cubic cell division. As the second test, backscatter RCS of a very thin lossy circular dielectric disk ($D = 1\lambda$ and $t = \lambda/50$) was computed with two different types of cells; a single-layer disk with $\lambda/20 \times \lambda/20 \times \lambda/50$ cells and a double-layer disk with $\lambda/20 \times \lambda/20 \times \lambda/100$ cells. Numerical results for these two cases are the same, which gives confidence on the MoM technique with very thin brick cells.

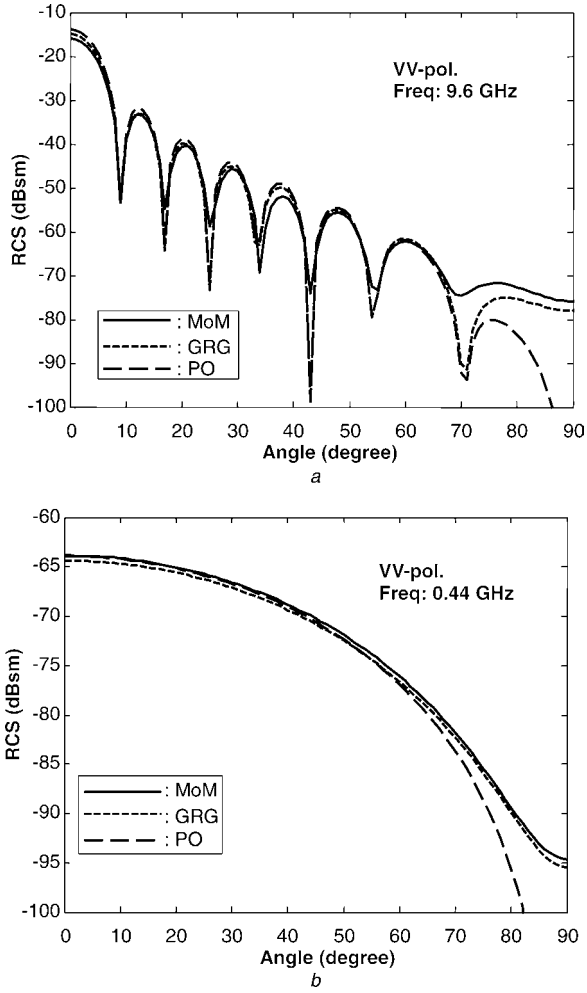

Fig. 4 *Comparison of analytical and numerical backscatter cross sections for VV-polarisation*

a 9.6 GHz
b 0.44 GHz

4 Comparison of models

The backscatter and forward-scatter RCSs are computed for a typical deciduous leaf for various frequencies and angles. A typical oak leaf is selected, as an example, which is an elliptical disk with a major axis of $2a = 12$ cm, a minor axis of $2b = 5$ cm, a thickness of $t = 0.02$ cm and a gravimetric moisture content of 0.6 g/cm^3, which corresponds to a complex dielectric constant as given in [14].

The backscattering cross sections of the leaf were computed using the GRG and PO approximations as well as the MoM for VV- and HH-polarisations over the range $0^\circ \leq \theta \leq 90^\circ$ at both 9.6 and 0.44 GHz. In these computations, the cell size of the elliptical dielectric disk for the MoM was 0.25×0.25 cm ($\lambda/12.5 \times \lambda/12.5$) which results in N (number of cells) = 741 at 9.6 GHz. Till now, it was commonly known that the GRG approximation holds for leaf surface dimensions smaller or comparable to the wavelength. However, Fig. 4*a* shows that the GRG approximation is as good as the PO approximation even for a large leaf with a leaf length of 3.84λ. Fig. 4*b* shows the backscattering cross sections of the dielectric disk at 0.44 GHz. In the MoM computation, the cell size was 0.4×0.4 cm ($\lambda/170 \times \lambda/170$) which gives $N = 297$ at 0.44 GHz. The length of the leaf is 0.176λ (=$\lambda/5.68$) at 0.44 GHz. Also, it was known that the PO approach is inherently a high-frequency approximation and therefore may be applied with caution when the size of a dielectric disk is not large compared with the wavelength [16]. Fig. 4*b*, however, shows that the PO approach is as good as the GRG approximation for a small elliptical dielectric disk with a length of 0.176λ. The PO model disagrees with the other models at large incidence angle ($\theta \geq 75^\circ$), near edge-on incidence, as shown in Figs 4*a* and *b*, because the disk is assumed as a surface-current sheet in the PO approximation. Similar results were also shown for HH-polarisation; the GRG and PO models are equally applicable for computation of the backscatter RCS of a thin dielectric disk at both frequencies (9.6 GHz corresponding to a leaf length of 3.84λ, and 0.44 GHz corresponding to 0.176λ).

Fig. 5*a* shows the forward-scattering cross sections of the leaf, which are computed using the analytical and numerical models at X-band for VV-polarisation. The incidence wave has $\theta_0 = 20^\circ$ ($\theta_i = 160^\circ$), $\phi_i = 0^\circ$ and the scattered wave has $\phi_s = 0^\circ$, $0^\circ \leq \theta_s \leq 180^\circ$ (Fig. 1). The GRG approximation for forward-scattering cross section agrees very well with the MoM even at 9.6 GHz, as in the backscattering case. The deviations of the forward-scattering cross sections computed by the GRG and PO models are less than 3 dB at most angles in comparison with the results of the MoM as shown in Fig. 5*a*, even for a large dielectric disk with a length of 3.84λ. The GRG and PO models also agree well with the MoM for HH-polarisation.

Fig. 5*b* demonstrates that the PO approach is also good for computing the forward-scattering cross section of the leaf even though the dimension of the leaf is very small

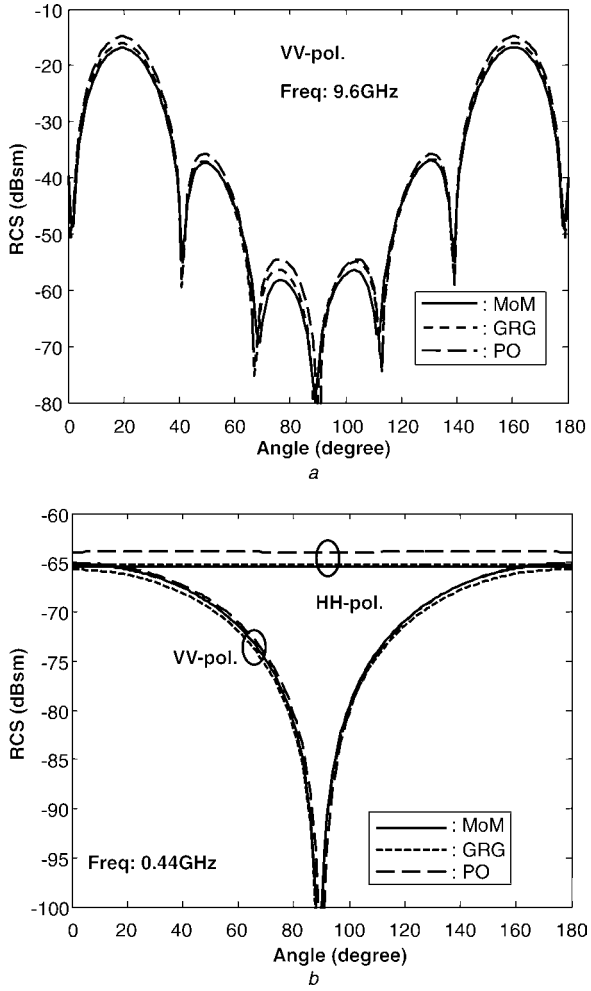

Fig. 5 *Comparison of analytical and numerical forward-scatter cross sections*

a 9.6 GHz, $\theta_o = 20^\circ$ for VV-polarisation
b 0.44 GHz, $\theta_o = 30^\circ$ for both polarisations

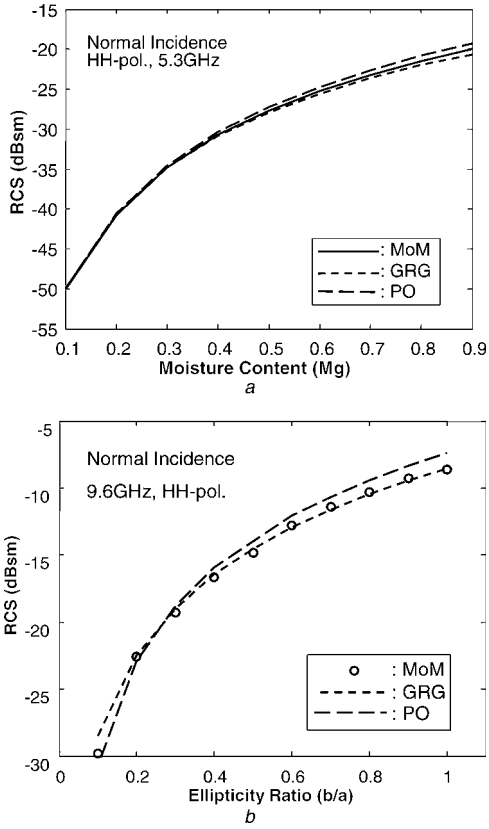

Fig. 6 *RCS as function of*

a Moisture content
b Ellipticity of the dielectric disk for backscatter at normal incidence and HH-polarisation

($2a = 0.176\lambda$ and $2b = 0.073\lambda$) compared to the wavelength at 0.44 GHz. The difference between the PO and the GRG models is less than 2 dB for both polarisations. The forward-scattering cross sections from those models agree well with that from the MoM for VV-polarisation, whereas PO model is about 1.5 dB higher than the MoM for HH-polarisation.

In order to generalise the results shown above, at first, the backscatter RCS of the dielectric disk with $2a = 12$ cm, $2b = 5$ cm and $t = 0.02$ cm was computed for various values of dielectric constants corresponding to various gravimetric moisture contents from 0.1 to 0.9 g/cm^3. Fig. 6*a* shows a typical example of the above computation results, for HH-polarisation, normal incidence at $f = 5.3$ GHz. Then, the backscatter RCS of the dielectric disk was computed for various shapes of the leaf, from an ellipse-shaped oblates ellipsoid with an ellipticity ratio of $b/a = 0.1$ to a circular-shaped oblate ellipsoid ($a = b$). Fig. 6*b* shows the computation results for HH-polarisation at 9.6 GHz. We obtained similar results for VV-polarisation and other frequencies. Therefore we can conclude that the GRG and PO models are equally applicable to the computation of the scattering matrix of a natural thin leaf at microwave frequencies for both polarisations regardless of the size, the moisture content and the shape of the leaf.

The computation time for a single leaf above was measured to estimate the complexity of each model. The GRG model took 0.029 s for the RCS computation of a single leaf using a PC with a 3 GHz CPU, whereas the PO model took 0.016 s. Therefore the PO model with the resistive sheet approximation is more efficient than the GRG model. The computation time for the MoM model depends on the number of cells; the example above took about 15 min with the same computer.

In reality, leaves are not of uniform thickness. Instead, natural leaves have randomly rough surfaces with very small roughness parameters: the RMS height and the correlation length. A randomly rough surface with small roughness parameters can be considered as an impedance surface with a surface impedance [17] of

$$\eta = -jZ_0 \frac{\sqrt{\pi}(ks)^2}{2kl} \tag{26}$$

where Z_0 is the intrinsic impedance of free space, k is the wavenumber, s is the RMS height and l is the correlation length of the rough surface. The difference between the RCS of the leaf with a uniform thickness and that with a small roughness is negligible (less than 0.0002 dB) at 9.6 GHz, normal incidence with $s = 0.001$ mm and $l = 1$ mm.

The forward-scatter and backwardscatter RCSs of the leaf for a range of thicknesses (0.1 mm $\leq t \leq$ 2.0 mm) at 9.6 and 0.44 GHz are computed using the GRG and PO models and the MoM for VV- and HH-polarisations. Figs 7*a* and *b* show the forward-scatter cross sections for thicknesses of 0.2 and 1.0 mm at $f = 9.6$ GHz and $\theta_0 = 30^\circ$ ($\theta_i = 150^\circ$) for VV-polarisation. The GRG and PO models agree very well with the MoM as shown in Fig. 7*a* for the thin disk case ($t = 0.2$ mm). However, Fig. 7*b* shows that the GRG and PO models deviate from the MoM because of a larger thickness. The thicker the

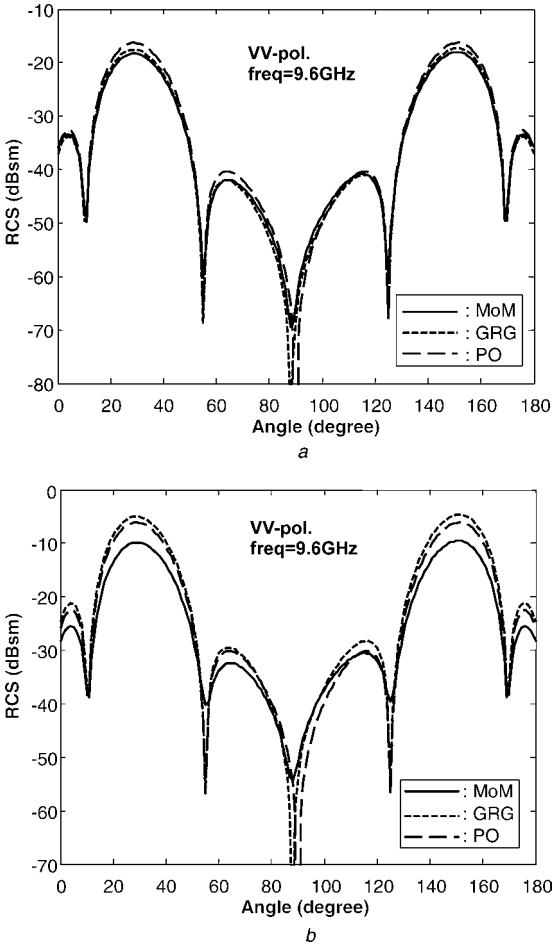

Fig. 7 *Forward-scatter cross sections at 30° and 9.6 GHz*
a $t = 0.2$ mm
b $t = 1.0$ mm.

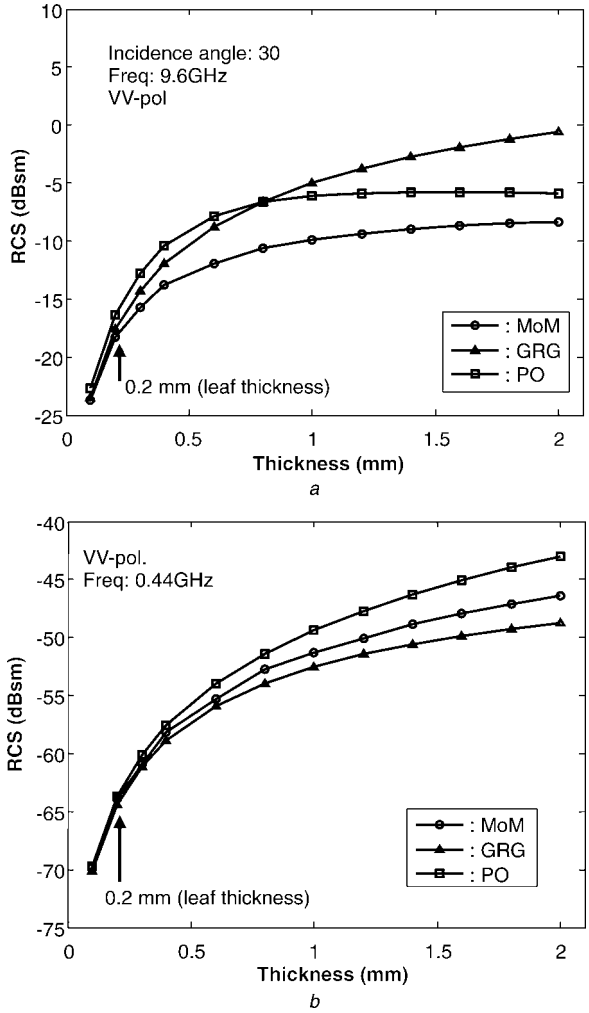

Fig. 8 *RCS of a leaf as a function of thickness at VV-polarisation*
a 30° forward-scatter at 9.6 GHz
b Normal incidence backscatter at 0.44 GHz

leaf is, the more deviation is expected between the GRG and PO models and the MoM.

Figs 8*a* and *b* show the numerical results as a function of thickness from 0.1 to 2.0 mm. The PO model agrees relatively well with the MoM even at large thickness, whereas the GRG model deviates much more from the MoM results at large thickness, at 9.6 GHz. Because the PO model employs the resistive sheet approximation, the accuracy of the PO model may be guaranteed only at the range of $k_0 t \ll 1$ [17]. Therefore Fig. 8*a* shows that the PO model deviates from the numerical solution at about $t \simeq 0.5$ mm and is saturated at $t > 1$ mm. Fig. 8*a* also shows that the analytical models agree with each other for small thicknesses ($t \leq 0.4$ mm) at 9.6 GHz for both polarisations. Fig. 8*b* shows the variation of the backscattering cross sections of the leaf as a function of thickness from 0.1 to 2.0 mm at 0.44 GHz for VV-polarisation, normal incidence ($\theta_0 = \theta_s = 0°$, $\theta_i = 180°$). The GRG and PO models agree relatively well with the MoM, especially at small values of thickness less than 0.5 mm at 0.44 GHz as shown in Fig. 8*b*. When we compute the scattering amplitudes of deciduous leaves having various sizes, shapes and orientations in a crown layer of vegetation canopy, we may choose either of the PO or of the GRG model regardless of the size of the leaves for practical range of microwave frequencies, because the thickness of the leaves is very small, $0.02 \leq t \leq 0.04$ cm. We could obtain similar results for other leaves with different shapes and different moisture contents.

Fig. 9 shows the backscattering cross sections at normal incidence ($\theta_0 = \theta_s = 0°$, $\theta_i = 180°$), for a leaf ($2a = 12$ cm, $2b = 5$ cm, $t = 0.04$ cm) over the frequency range of $0.25 \text{ GHz} \leq f \leq 25$ GHz, which corresponds to the leaf length range of $0.1\lambda \leq 2a \leq 10\lambda$ for VV-polarisation. The difference between the PO and the GRG models is less than 2 dB over the range $0.1\lambda \leq 2a \leq 10\lambda$ as shown in Fig. 9. The angular variations

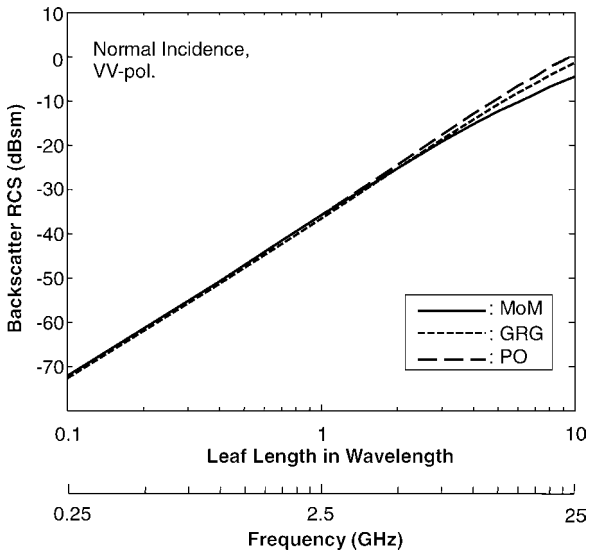

Fig. 9 *Variation of the backscatter RCS as a function of frequency at normal incidence for VV-polarisation*

of both models are identical, because the modifying factors of both models have the same angular variations as in (9), (12) and (16). This result informs us that the GRG and PO models are equally applicable to compute the scattering matrix of a natural deciduous leaf at microwave frequencies; that is, the GRG model is as good as the PO model for computation of the scattering amplitudes of leaves ten times larger than a wavelength, and on the other hand, the PO model is as good as the GRG model for leaves 0.1 times smaller than a wavelength.

5 Conclusion

The accuracies of the GRG and PO models for scattering from deciduous leaves (very thin lossy dielectric disks) were investigated based on the precise numerical results of the MoM. It was found that the GRG and PO models extend their validity regions for scattering amplitudes as the thickness of a lossy dielectric disk decreases. Both models agree quite well with the precise MoM results for scattering from natural deciduous leaves, because the thickness of the leaves is very small, $0.02 \leq t \leq 0.04$ mm. It was also found in this study that both the GRG and PO models could be used for computing the scattering amplitudes of the leaves over the range of length $0.1\lambda \leq 2a \leq 10\lambda$ (corresponding to the range of frequency 0.25 GHz $\leq f \leq$ 25 GHz for a leaf with a length of 12 cm as an example). It can be recommended that both the PO and GRG models be alternatively used for computing the scattering matrices (or the phase matrices) of natural deciduous leaves (included in a vegetation canopy) at microwave frequencies.

6 Acknowledgments

The authors wish to thank the anonymous reviewers for their thoughtful comments. The authors also thank Saeroonter Oh for his proof-reading of this manuscript. This work was supported by the Korea Agency for Defense Development, through the Radiowave Detection Research Center at KAIST, and grant R01-2005-000-10101 from the Basic Research Program of the Korea Science and Engineering Foundation.

7 References

1 Ulaby, F.T., Sarabandi, K., McDonald, K., Whitt, M., and Dobson, M.C.: 'Michigan microwave canopy scattering model', *Int. J. Remote Sensing*, 1990, **11**, (7), pp. 1223–1253
2 Karam, M.A., Fung, A.K., Lang, R.H., and Chauhan, N.S.: 'A microwave scattering model for layered vegetation', *IEEE Trans. Geosci. Remote Sensing*, 1992, **30**, (4), pp. 767–784
3 Richter, J., Caldeirinha, R.F.S., AL-Nuaimi, M.O., Seville, A., Rogers, N.C., and Savage, N.: 'A generic narrowband model for radiowave propagation through vegetation'. Proc. IEEE Vehicular Technology Conf., Stockholm, Sweden, June 2005, vol. 1, pp. 39–43
4 Senior, T.B.A., Sarabandi, K., and Ulaby, F.T.: 'Measuring and modeling the backscattering cross section of a leaf', *Radio Sci.*, 1987, **22**, (6), pp. 1109–1116
5 Karam, M.A., Fung, A.K., and Antar, Y.M.M.: 'Electromagnetic wave scattering from some vegetation samples', *IEEE Trans. Geosci. Remote Sensing*, 1988, **26**, (6), pp. 799–808
6 Pan, G., and Narayanan, R.M.: 'Electromagnetic scattering from a dielectric sheet using the method of moments with approximate boundary condition', *Electromagnetics*, 2004, **24**, (5), pp. 369–384
7 Pan, G., and Narayanan, R.M.: 'Correction to "electromagnetic scattering from a dielectric sheet using the method of moments with approximate boundary condition"', *Electromagnetics*, 2005, **25**, (2), pp. 169–176
8 Oh, Y., Jang, Y-M., and Sarabandi, K.: 'Full-wave analysis of microwave scattering from short vegetation: an investigation on the effect of multiple scattering', *IEEE Trans. Geosci. Remote Sensing*, 2002, **40**, (11), pp. 2522–2526
9 Ulaby, F.T., and Elachi, C.: 'Radar polarimetry for geoscience applications' (Artech House, 1990, 1st edn.)
10 Tai, C.T.: 'Dyadic Green's functions in electromagnetic theory' (Intext Educational Publishers, 1971, 1st edn.)
11 Karam, M.A., and Fung, A.K.: 'Leaf-shape effects in electromagnetic wave scattering from vegetation', *IEEE Trans. Geosci. Remote Sensing*, 1989, **27**, (6), pp. 687–697
12 Tsang, L., Kong, J.A., and Shin, R.T.: 'Theory of microwave remote sensing' (John Wiley and Sons, 1985, 1st edn.)
13 Abramowitz, M., and Stegan, I.A.: 'Handbook of mathematical functions' (Dover Publication, Inc., 1972, 1st edn.)
14 Ulaby, F.T., and El-rayes, M.A.: 'Microwave dielectric spectrum of vegetation – Part α: Dual-dispersion model', *IEEE Trans. Geosci. Remote Sensing*, 1987, **25**, pp. 550–557
15 Sarkar, T.K., Arvas, E., and Ponnapalli, S.: 'Electromagnetic scattering from dielectric bodies', *IEEE Trans. Antennas Propag.*, 1989, **37**, pp. 673–676
16 Le Vine, D.M.: 'The radar cross section of dielectric disks', *IEEE Trans. Antennas Propag.*, 1984, **32**, (1), pp. 6–12
17 Senior, T.B.A., and Volakis, J.L.: 'Approximate boundary conditions in electromagnetics' (IEE Press, 1995, 1st edn.)